Dual Differential Rheological Actuator for High Performance Physical Robotic Interaction

Philippe Fauteux, *Student Member*, *IEEE*, Michel Lauria, *Member*, *IEEE*, Benoît Heintz and François Michaud, *Member*, *IEEE*

***Abstract*—Today's robotic systems are mostly rigid and position controlled machines designed to operate in structured environments. To extend their application domains to partially unknown, dynamic or anthropic environments, improved physical interaction capabilities are required. In this new context, blending in the requirements for safety, robustness and versatility is often challenging in part because commonly available actuator technologies are inadequate. This paper presents our solution by introducing the Dual Differential Rheological Actuator (DDRA) concept based on the synergistic combination of an electromagnetic motor and two differentially coupled magnetorheological brakes. This paper describes the approach and the prototype design. It then discusses performances in force, motion and interaction control.**

***Index Terms*—Actuators, force and interaction control, human-robot interaction, low impedance actuation, soft robotics.**

I. Introduction

ROBOTS and humans share complementary skills, which suggests we could benefit from an increased level of collaboration. Robots possess speed, precision, strength and can handle dangerous, strenuous or tedious tasks without being subject to injuries or fatigue. Humans, on the other hand, are unmatched in their ability to perceive and to interpret, providing global understanding and guidance.

However, the reality is that current robotic manipulators, faithful to their roots in the 1950s, are still mostly stiff and position controlled machines fundamentally incompatible with this scenario. Indeed, in the broad context of physical interaction, robots remain somewhat clumsy. Despite impressive motion performances, they struggle to control the interaction force with precision and high bandwidth. Also, they do not handle collisions graciously and are generally bad at interacting with partially unknown or kinematically constrained environments. As a result, their applicability remains generally bounded to simple motion tasks in highly structured environments.

For a number of applications, the need for high-force, safe, robust and versatile robots physically interacting with their environment and going beyond simple position control is yet to be adequately supported. Such capabilities are sought-after to improve the performance of industrial robots in tasks such as assembling, polishing, deburring and machining [1]. They could also enable robots to work side-by-side with operators, leading to reduced programming times and to more efficient and flexible assembly lines [2][3]. In addition, robotic systems with such capabilities could increase the effectiveness and efficiency of physical rehabilitation therapy by delivering consistent treatments and by providing an objective tracking of progress [4][5]. Moreover, such technologies could ease the design of manipulators for assistive robots and of motorized orthesis-prosthesis [6]-[8].

For these reasons, robot force and interaction control is receiving growing interest in the field. One approach is to use available robots, equip them with an end-effector force sensor, and perform closed-loop control [1][3]. Typically, however, performances remain limited because of high effective impedance and low controllable force bandwidth. One solution to the limitations of current designs lays in developing actuation methods better suited to the new set of requirements relevant to interactive robotics. The Dual Differential Rheological Actuator (DDRA) was developed to address this issue. This technology is based on the synergistic use of an electromagnetic (EM) motor and two differentially coupled magnetorheological (MR) brakes. Contrasting with most actuators, this combination makes possible the simultaneous achievement of high force density, low intrinsic impedance, high force bandwidth and high precision force control which, we believe, enables safe, robust and highly versatile physical interactions.

The paper is organized as follows. Section II presents important considerations for interactive robotics. Section III

Manuscript received December 4, 2009. This work was supported in part by the Natural Sciences and Engineering Research Council of Canada and the Canada Council for the Arts. Patent pending PCT/CA2009/000390.

This paper has supplementary downloadable material available at http://ieeexplore.ieee.org. This includes a M4V (QuickTime) format movie clip, which shows the prototype performing force, interaction and motion control tasks. This material is 23 MB in size.

P. Fauteux is with the Department of Mechanical Engineering, Université de Sherbrooke, Sherbrooke, Québec Canada J1K 2R1 (corresponding author, phone: 819 821-8000, Extension 62893; fax: 819 821-7937; e-mail: philippe.fauteux@usherbrooke.ca).

M. Lauria is with University of Applied Sciences Western Switzerland (HES-SO), Geneva, Switzerland (email: michel.lauria@hesge.ch).

Benoît Heintz and François Michaud are with the Department of Electrical Engineering and Computer Engineering, Université de Sherbrooke, Sherbrooke, Québec Canada J1K 2R1 (email: {benoit.heintz, francois.michaud}@usherbrooke.ca.)

discusses how actuators can contribute to address these considerations. Sections IV and V describe the DDRA concept and its implementation in a prototype. Section VI presents force, interaction and motion control results. Section VII discusses the observed performances using EM motors as comparatives. Concluding remarks are given in Section VIII.

II. Considerations for Interactive Robotics

Building robots interacting successfully in poorly defined, dynamic or anthropic domains is challenging. This section discusses the issues of safety, robustness and versatility.

A. Safety

Physical interaction in anthropic domains creates obvious safety concerns which have been the subject of much research and debate [9][10]. Hazards particularly arise when interaction forces are not limited to acceptable levels such as during collision or clamping events. In the case of a static clamping, the potential for injury is mainly defined by the maximum force the robot is able or allowed to exert, which is controllable. In the case of a dynamic collision or clamping however, the kinetic energy of the robot represents a serious and hard to manage threat. Indeed, a recent test and simulation campaign demonstrated that the dynamic clamping of an operator head by a small robot moving at a typical speed can cause a fracture of the frontal bone (4 kN impact force) even if maximum reverse torque is applied instantly on contact [11].

This risk level must obviously be reduced. A few approaches are possible. Undesired collision occurrences can be decreased through sensorisation and reactive control schemes. The robot then monitors the human actions and stops moving, reduces its speed or modifies its trajectory when required. Depending on the desired level of intimate contact and collaboration, this might not always be applicable or sufficient. Then, compliant coverings can be added to reduce the magnitude of impact forces, although impractically large amounts of material may be necessary for typical industrial robots [12]. The root of the problem remains the amount of kinetic energy of the moving robot, which can only be lessened either by decreasing velocity or by decreasing the effective inertia. The former is easy to implement, but limits the ability to produce useful work. The latter, unfortunately, is not trivial.

B. Robustness

In robotic manipulators, motion tracking controllers, high impedance actuators and stiff transmissions team up to reject force disturbances. These fundamental building blocks, useful for high performance motion, are nonetheless incompatible with robust interaction in kinematically constrained environments. For instance, within this design paradigm, tasks as simple as opening a drawer or a door become very challenging because any inaccuracy in motion creates large reaction forces which threaten the integrity of the robot and the environment. Actions must thus be performed slowly and carefully while a high burden is put on modeling and control.

A kinematic constraint imposes restrictions on allowed trajectories. The only way to gracefully and non-destructively handle tasks is then to accept and give way under those constraints. One approach is to use an end-effector force sensor mounted on a stiff robot and to add compliance by control. However, because controllers and actuators have limited power and bandwidth, the compliant control of stiff architectures is only possible at low frequencies. This is hardly compatible with fast interactions with partially unknown or kinematically constrained environments. Intrinsic robustness demands low intrinsic inertia and sufficient open-loop backdrivability.

C. Versatility

Bodies physically interact when, once coupled, they exchange mechanical energy through the flow of two conjugate variables: force and velocity. Versatility in interaction could be defined as an ability to control those variables in a manner that enables the competent carrying out of a broad diversity of tasks. Consider, for example, the case where a robot must allow the motion of a user, but only through a predefined path. The successful completion of this task suggests that a possibly complex set of relationships controls the dependence of force to motion, or vice-versa, during the interaction.

Traditional robotics focuses on imposing velocity using motion feedback. This is suited only for a limited number of tasks. A more general approach, termed interaction or impedance control, consists in regulating the dynamic relationship between the two interaction variables at the ports of interaction [13][14]. Within this behavioural tracking paradigm, the definition of performance is extended to include the ability to stably and precisely emulate a wide range of impedances over a large frequency spectrum [15][16]. Besides increased versatility, interaction control has advantages regarding stability analysis for interaction with unknown environments. Traditional stability analyses require knowledge of the plant to be controlled. However, because most environments are passive, the coupled stability can usually be guaranteed as long as the emulated impedance is passive [17].

The control tools for stable and versatile interaction thus exist. However, once again, the hardware of classic robots poses serious limitations. Because a controller and actuator have limited power and bandwidth, it will always be difficult to emulate low impedances with high impedance robots. On a more theoretical basis, because of the finite structural stiffness of robots, using control to mask more than about half of the intrinsic inertia typically trespasses the passivity criteria, leading to a potential for coupled instabilities [18][19]. This advocates again for low inertia hardware. On the other hand, with low impedance hardware, a large force bandwidth is necessary to emulate high impedances. Both are thus necessary for highly versatile interactions.

III. Actuators for Interaction Control

Based on the issues of safety, robustness and versatility, actuators designed for interactive robotics should have the following capabilities, which are somewhat competing:

1) *High torque density.* For serial structures with actuators collocated with joints, it enables the design of lighter and lower inertia robots.
2) *Low intrinsic output impedance.* Inertia is detrimental because it creates undesired dynamic interaction forces. Joint friction is also undesirable because it inhibits joint backdrivability which can reduce the magnitude of these undesired forces.
3) *High bandwidth force control.* This is required to achieve fast and stiff motion control or to enable the stable emulation of high impedances with low impedance hardware.
4) *Precise force control.* The ability to generate a given force with high fidelity is desirable in a number of force and interaction control tasks.

Common actuators do not simultaneously achieve these four requirements as illustrated in Fig. 1, where requirements 2 to 4 are combined into the "aptitude to force control" criteria [20]. The force density of direct drive EM motors is often insufficient. It is typically limited to somewhere between 2.5 and 6 Nm/kg for convection cooled, torque optimized and frameless motors [21]. Then, the force control aptitude of geared motors is usually too low. This is the result of the transmission backlash, non-linear friction and elasticity. Their intrinsic inertia is also high because of the speed reduction transmission inertia multiplying effect. As a reference, this speed reduction ratio is often chosen so that the effective inertia of the actuator roughly matches that of the actuated link with its load in order to optimize dynamic performances and reduce control instabilities [22]. Also, because of the compressibility of air, the bandwidth of pneumatic actuators is typically insufficient to provide a generalizable solution. Finally, by their nature, flow controlled hydraulic actuators have too much impedance.

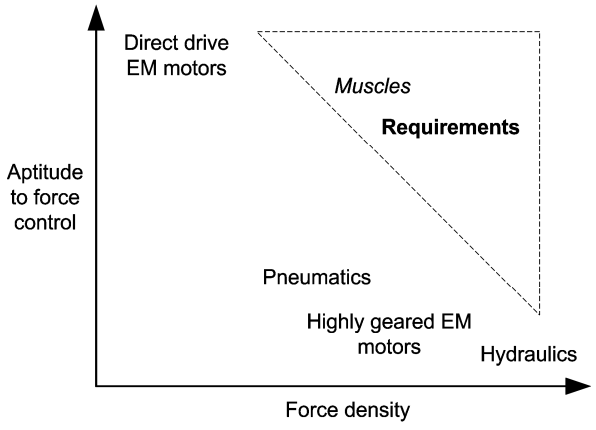

Fig. 1. Aptitude to force control versus force density for common actuators.

To compensate for these limitations, actuators specifically designed for interaction have been proposed:

Relocated Direct Drive Motors. Direct drive motors are attractive because they are usually low inertia and low friction devices with a known relationship between the winding current and the output force. Fast, precise and inherently stable force control can thus be achieved using a current feed-forward scheme. However, because of mass and weight constraints, it is often desirable to relocate them near the robot base. Mechanical power must then be conveyed through stiff and efficient transmissions, which can be a challenge to design and integrate. The MIT-Manus rehabilitation device sold by Interactive Motion Technologies and the Whole Arm Manipulator sold by Barrett Technologies are examples of designs using this approach [23][24].

Force Feedback Actuators. These actuators are composed of high force density actuators, such as geared EM motors, equipped with an output force sensor to enable closed-loop force control [25]. However, the non-collocation of the sensing and actuating transducers and other factors (e.g., limited sampling frequencies) limit stable feedback gains and stable control bandwidth [18][26]. Above this bandwidth, the open-loop dynamics invariably dominates and can pose a threat to safety and robustness. One of the foremost initiatives using this method was undertaken by the German Aerospace Center (DLR) and resulted in three generations of extensively optimized lightweight robotic arms [27]. Performances are impressive but robustness is still an issue [28].

Series & Differential Elastic Actuators (SEA & DEA). To improve the safety and robustness of Force Feedback Actuators, a compliant element is placed at the output. This enhances force resolution, control stability and impact tolerance [29]-[31]. However, the introduced flexibility limits the efficiency with which power is transferred from the transducer to the link. This results in a drop of controllable bandwidth. SEA have been used in walking and running robots, motorized prosthesis-orthesis, rehabilitation devices and a few interactive manipulators such as for Domo from the Massachusetts Institute of Technology [32]. DEA are used for the locomotion of an omnidirectional wheel/track robot [31].

Parallel Coupled Micro-Macro Actuators. To improve the force control bandwidth of a SEA, a low power direct drive motor is added in parallel. The SEA generates low frequencies and high amplitude forces whereas the direct drive motor contributes for high frequencies and low power forces [33]. To reduce the moving mass, the SEA can be relocated near the robot base whereas the direct drive motor remains collocated with the joint. This is referred to as the Distributed Macro-Mini Actuators approach [12]. The direct drive motor extends bandwidth and thus performances. This nonetheless comes at the price of increased volume, mass and complexity. The distributed approach has recently been used to create a large workspace haptic interface [34]. Willow Garage PR2 platform also uses this approach, but with the SEA being connected to a more intricate gravity compensation mechanism [6].

Variable Stiffness Actuators. A Variable Stiffness Actuator could be described as a SEA with an actuated mechanism enabling a real time variation of the compliant element stiffness. With this method, motion performance while operating under safety constraints is improved by combining low velocity with high stiffness and high velocity with low stiffness, where low stiffness provides a better isolation from the motor inertia [35]-[37]. Another important advantage is that the mechanically rendered stiffness is not subject to a loss of passivity. The drawbacks of current designs include

mechanical complexity, time delays for stiffness modulation and limited stiffness ranges.

Actuators with Clutch. These actuators use a force controllable clutch placed between a high force density actuator (the velocity source) and the load [38][39]. Advantageously, the clutch isolates the environment from the inertia of the velocity source. On the other hand, the intrinsic clutch friction can limit the ability to control small forces accurately. Also, because the direction of the velocity slippage in the clutch must always correspond to the direction of the desired interaction force, the bandwidth around zero force is tributary of the velocity source performance.

Dual Clutches Actuators. These actuators are built by connecting the outputs of two force controllable clutches being driven in opposite directions. This proposition was made in contexts ranging from haptic displays to high performance motion [40]-[43]. Indeed, this approach has several interesting consequences: these actuators display very low output impedance and no backlash and, depending on the clutch technology, can be able of fast and precise open-loop force control. Nevertheless, mechanical integration remains a challenge and the resulting prototypes are bulky.

IV. Dual Differential Rheological Actuator

Designing actuators suited for high force physical interaction is not trivial. Indeed, because of conflicting requirements and limited design options, most approaches still struggle to deliver high performance in convenient packages. Our actuation solution, thereby identified as the Dual Differential Rheological Actuator (DDRA), is based on the synergistic use of two differentially coupled MR brakes and an EM motor. This configuration shares similarities with the Dual Clutches Actuators. However, the differential configuration solves a number of integration issues. This section describes the DDRA concept starting with MR brakes and mechanical differentials, which are important building blocks.

A. Magnetorheological Brakes

MR fluids are typically composed of micro-sized ferromagnetic particles mixed in a carrier liquid. When a magnetic field is created in the fluid, the magnetisable particles align and form columns. These columns oppose motion up to a shear stress threshold determined by the intensity of the field, at which point the fluid starts to flow [44][45].

This principle is exploited in MR brakes, which use one or a plurality of interspersed rotor and stator blades to shear the fluid, as shown in Fig. 2. Multiple blades increase the shear area and make it possible to produce large forces. Fig. 3 shows typical braking torques T_B versus angular velocity ω for different magnetic field strengths H. B_B is the brake drag coefficient due to fluid viscosity. A stiction phenomenon is visible at low speeds. Nevertheless, if there is motion between blades, the output torque can be approximated as (1), describing a plastic Bingham model with an added dry friction coefficient T_f. This friction can be attributed, for example, to sealing elements. In this model, the fluid viscosity is considered to be independent of velocity, although shear rate thinning is usually reported [46]. In a typical MR brake, the field dependant yield torque $T_y(H)$ is controlled by modulating the current flowing through the coil [47]-[49].

To help explain the DDRA mechanism, rotational to linear analogies are provided later on. For this reason, a linear equivalent of (1) is given in (2), where F_B is the braking force, $F_y(H)$ is the controllable field dependant yield force, F_f is the dry friction force, v is the velocity and C_B is the damping coefficient.

$$T_B = (T_y(H) + T_f)\,\mathrm{sgn}(\omega) + B_B\omega \quad (1)$$

$$F_B = (F_y(H) + F_f)\,\mathrm{sgn}(v) + C_B v \quad (2)$$

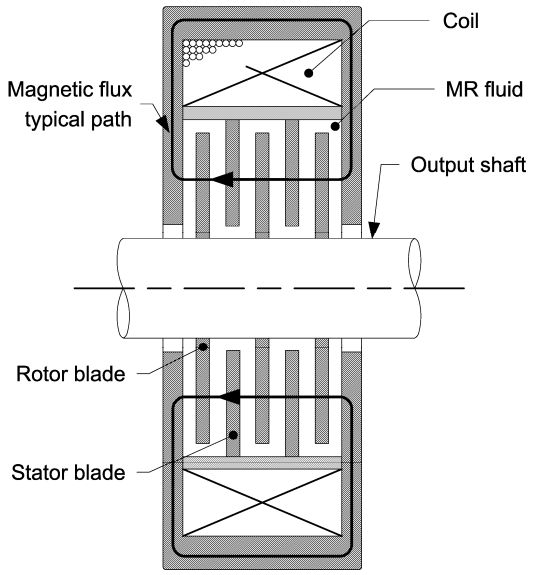

Fig. 2. Cross-sectional view of a typical magnetorheological brake.

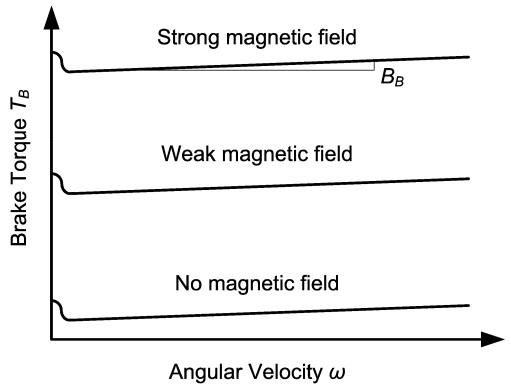

Fig. 3. Typical magnetorheological brake torque versus angular velocity for different magnetic field strengths.

Well-designed MR brakes display high torque density, very low inertia, high bandwidth and low power consumption. Drawbacks possibly include a hysteretic torque to current relationship caused by magnetic remanence [50]. The consistency of this relationship can also be affected by gravitational particle settling, magnetic gradient induced particle migration or particle centrifugation phenomena [51][52]. Well formulated fluids and good brake designs are thus required.

B. Mechanical Differentials

Mechanical differentials are mechanisms possessing three ports among which force or torque is distributed following a known relationship. The lever mechanism illustrated in Fig. 4 is an example used here as an analogy to all other differential mechanisms. This lever has three ports (O_1, O_2 and O_3) to which external forces (F_1, F_2 and F_3) are applied. To assess the effects of the mechanism inertia, a lumped mass (m_1, m_2 or m_3) is associated to each port. For this configuration, the kinematic relationship between port velocities (v_1, v_2 and v_3) is expressed using the Willis formula (3). Force relationships, derived using basic dynamics, are expressed in (4).

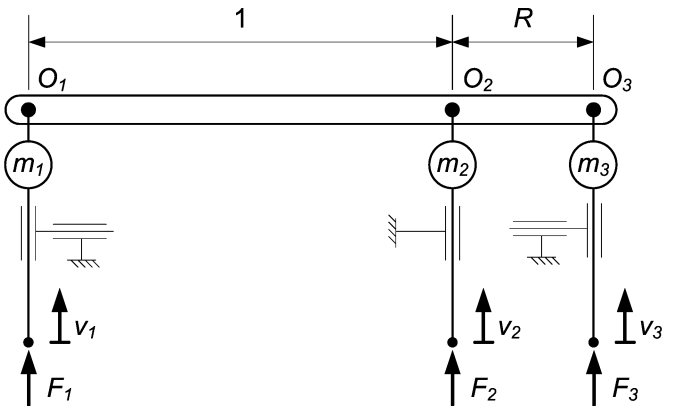

Fig. 4 Lever in a differential configuration with added lumped masses.

$$v_3 + Rv_1 = (1+R)v_2 \tag{3}$$

$$\begin{cases} F_1 = F_3 R - \dot{v}_3 R m_3 + m_1 \dot{v}_1 \\ F_2 = -F_3(1+R) + \\ \qquad + \dot{v}_2(m_2 + (1+R)^2 m_3) - \dot{v}_1((1+R)Rm_3) \end{cases} \tag{4}$$

C. DDRA Concept

The DDRA makes use of two differentially coupled MR brakes to control the flow of mechanical power from a velocity source to the load. The configuration is such that the interaction force can be controlled, in both directions, by a combination of the two braking forces.

Such a configuration is schematically illustrated in Fig. 5, using the lever analogy. The velocity source (not shown) moves the ports O_1 and O_4 at velocity v_{in} in opposed directions. Pivots O_3 and O_6 are respectively connected to mechanically grounded brakes 1 and 2 which resist motion with forces F_{B1} and F_{B2} modeled using (2). Pivots O_2 and O_5 are linked together and form the actuator output. Lumped masses (m_{in}, m_B and m_{out}) are added to consider inertial effects. m_{in} represents half the inertia of the velocity source and of a fraction of the differential mechanism. m_B symbolizes the inertia of a brake and of a fraction of the differential mechanism. m_{out} finally stands for the inertia of the output link and of the remaining portions of the differential mechanisms.

Consider the case where both brakes are similar: same damping coefficients and same dry friction forces. Also, consider that the input velocity v_{in} is sufficient to ensure that, despite output motion v_{out}, ports O_2 and O_5 are moving in opposite directions. The interaction force F_{out} can then be expressed as in (5), derived using (2) and (4). This relationship shows that the output force is strictly a linear combination of the two open-loop controllable field dependant yield forces of the brakes ($F_{y1}(H_1)$ and $F_{y2}(H_2)$ for brakes 1 and 2) and of the dynamic effects of the intrinsic impedance $Z_{out}(s)$, where s is the Laplace complex argument.

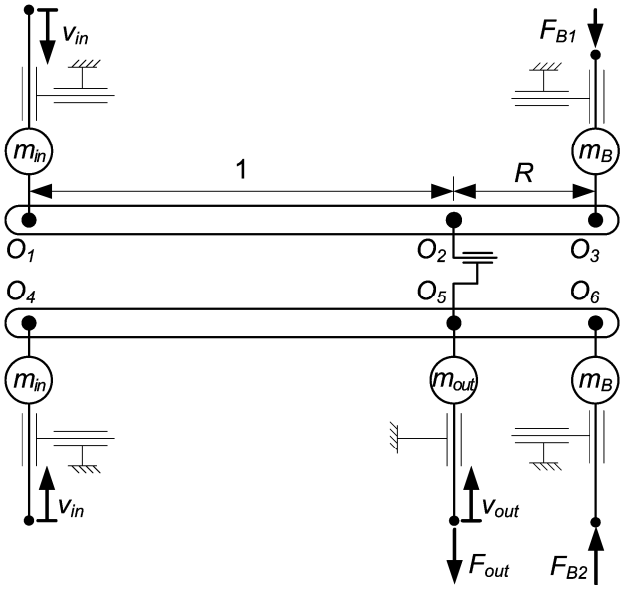

Fig. 5 Schematic lever analogy of a DDRA configuration.

$$\begin{cases} F_{out} = F_C - v_{out}(s) Z_{out}(s) \\ F_C = (F_{y2}(H_2) - F_{y1}(H_1))(1+R) \\ Z_{out}(s) = 2(1+R)^2 (m_B s + C_B) + m_{out} s \end{cases} \tag{5}$$

Many advantages come with the DDRA concept:

- Output inertia is exceptionally low because it is decoupled from the velocity source as illustrated by (5), where $Z_{out}(s)$ is not a function of m_{in}.
- Output friction is small. Because of symmetry in the design, the brakes dry friction forces oppose each other and tend to cancel themselves out. Concerns regarding brake stiction are also eliminated because ports O_3 and O_6 are in continuous motion.
- Forces can be controlled over a large bandwidth by making use of fast brakes. Very little detrimental elasticity is introduced between the brakes and the output.
- High-fidelity force control is possible. In geared motors, the transmission adds a lot of noise on the output force. The proposed concept links the brakes to the output through minimal gearing.
- Backlash is eliminated by the opposition of internal forces. This improves positioning precision and enables a high inertia mismatch between the actuator and the load without compromising the stability of motion controllers.

- The interaction force can be controlled without a torque sensor simply by modulating the currents in the brakes. This feed-forward approach is inherently stable.
- The design is robust and impact tolerant. The output force remains under control even during collisions. The excess energy is simply dissipated in the brakes.
- The velocity source can be implemented with low grade components. Because the brakes control the interaction, there are no stringent performance requirements for the velocity source. Its gearing can furthermore be fabricated with backlash and kinematic imperfections without affecting performances.

D. Proof-of-Concept Prototype

Before initiating the design of a complete custom-built DDRA, we first validated the concept using standard MR brakes [53]. Fig. 6 shows an exploded view of the actuator mechanism. Fig. 7 shows the actuator with its output connected to a torque sensor for characterization purposes.

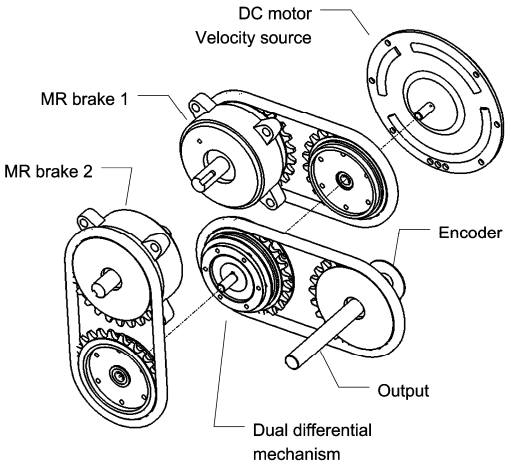

Fig. 6 Exploded view of the proof-of-concept prototype mechanism.

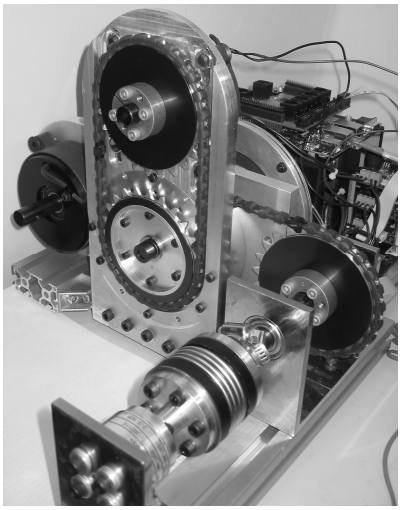

Fig. 7 Image of the proof-of-concept prototype.

V. IMPLEMENTATION

Fig. 8 illustrates and describes the hardware of our first complete and integrated DDRA prototype. It consists of a velocity source, two MR brakes, a dual differential mechanism and drive electronics with a position feedback device.

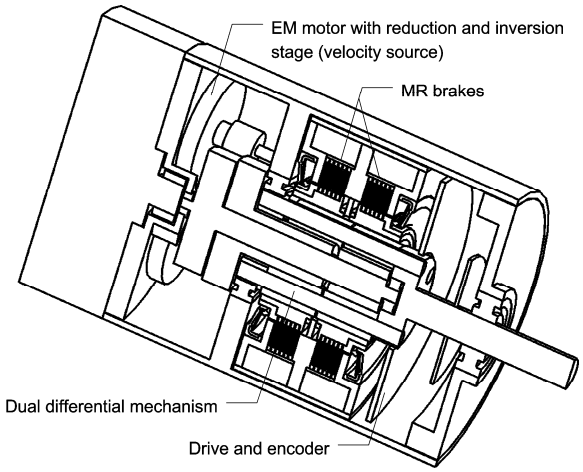

Fig. 8 Cross-sectional view of the DDRA prototype.

The velocity source includes a brushless DC motor and a geared velocity reduction and inversion stage. More details are visible in the exploded view of Fig. 9 where arrows indicate rotation directions. The output gears O_1 and O_4, where numbers refer to Fig. 5, are the inputs of the dual differential mechanism. They rotate with the same velocity (ω_{in}) but in opposite directions.

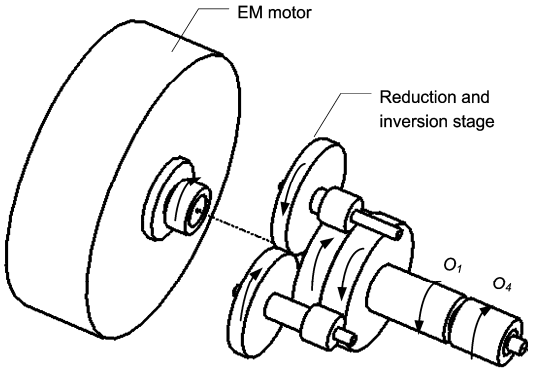

Fig. 9 Exploded view of the velocity source.

The MR brakes module is shown in Fig. 10. When a current flows in a coil, a magnetic flux is created in the corresponding brake which starts resisting motion. By modulating currents (I_1 and I_2 for brakes 1 and 2), the field dependant braking torques ($T_{y1}(H_1)$ and $T_{y2}(H_2)$) are controlled. The rotors of brakes 1 and 2 are respectively mounted on internal gears O_3 and O_6.

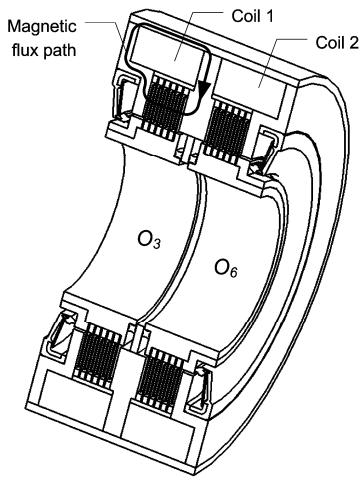

Fig. 10 Cross-sectional perspective view of the MR brakes module.

Two epicyclic gearing stages are used to create the dual differential mechanism. An epicyclic gearing stage, in a differential configuration, is equivalent to the lever of Fig. 4 with R being the ratio of sun gear to annulus gear numbers of teeth. The sun gear is port O_1, the planet carrier is port O_2 and the annulus gear is port O_3. A simplified exploded view of the dual differential mechanism is presented in Fig. 11. Ports O_1 and O_4 are connected to the velocity source whereas ports O_3 and O_6 are connected to brakes. A single planet carrier guides the planetary gears of both stages and forms the output.

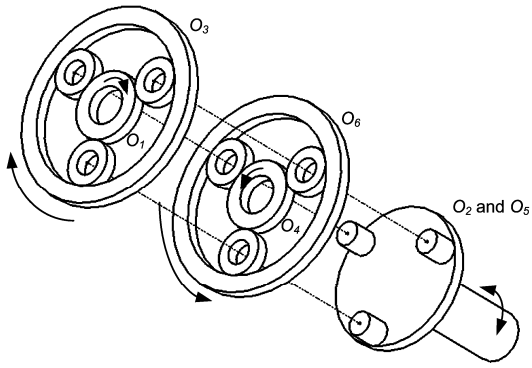

Fig. 11 Exploded view (simplified) of the dual differential mechanism.

A position feedback device, a controller and the drive electronics are included within the actuator main volume. The purpose of the controller is twofold: it commands the velocity source and controls the current supplied to the brakes to produce the desired behavior. The velocity source is controlled through a classic PID feedback loop using information from the motor Hall effect sensors. For the output force or torque to be described using (5), the input velocity must be sufficient. The input velocity reference ($\omega_{in\text{-}ref}$) is thus set using (6) where R is the dual differential mechanism reduction ratio (see Fig. 5), ω_{out} is the output velocity and ω_m is a velocity margin. This margin is used to circumvent the dynamic performance limitations of the motor when high accelerations are expected. It can be chosen and varied according to the task.

$$\omega_{in-ref} = \left|\omega_{out}\right| R + \omega_m \tag{6}$$

VI. Results

Table I presents the specifications of our DDRA prototype. Its intrinsic impedance can be estimated using CAD tools and simple models: it is a combination of a small inertia and a small damping. In this section, performances are evaluated in the contexts of torque, interaction and motion control.

TABLE I
DDRA Prototype Specifications

Dimensions	90 mm diameter by 137 mm
Mass	2.4 kg
Maximum torque	20 Nm
Nominal torque (estimate)	11 Nm
Maximum velocity	160 rpm (with 37 V power supply)
Nominal power output (estimate)	150 W (with 37 V power supply)
Output inertia (estimate)	$1.2e^{-4}$ kg.m^2
Output damping (estimate)	0.01 Nm.s/rad

A. Torque Control

With the DDRA prototype, torque control was performed using a current feed-forward approach, which required knowledge of brake currents versus output torque relationships. To identify them, the following experiment was conducted. The actuator output was coupled to a fixed torque sensor as shown in Fig. 12. The velocity source was set to rotate and a slowly varying sinusoidal current was sent to a brake, then to the other. Current commands and measured torques were recorded over several sinusoid periods by the microcontroller of the drive. This data was communicated to a PC using a CAN to USB converter. Because output velocity is zero, the intrinsic impedance $Z_{out}(s)$ has no effect on the output torque. What is measured is thus the open-loop controllable torque T_C (F_C in (5)). Data and fitted third order polynomial functions are presented in Fig. 13. At zero current, both curves cross at a small torque value identified as T_0. Fig. 14 gives a closer view of the torque generated by brake 1 over one sinusoid period. This information is filtered with a 10 Hz cutoff frequency to reveal a small hysteresis.

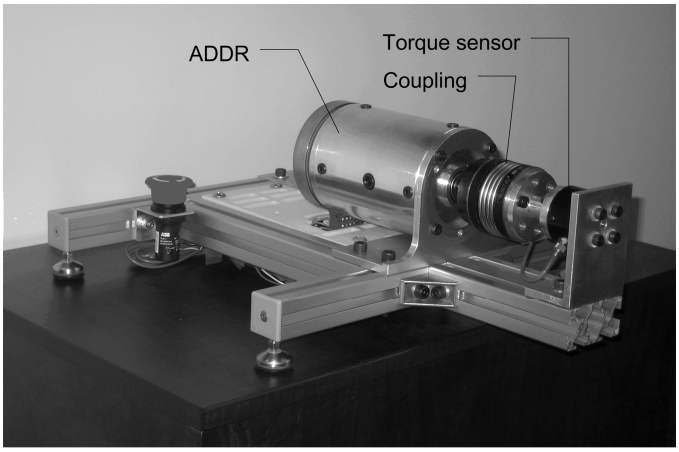

Fig. 12 Experimental setup to measure the static output torque.

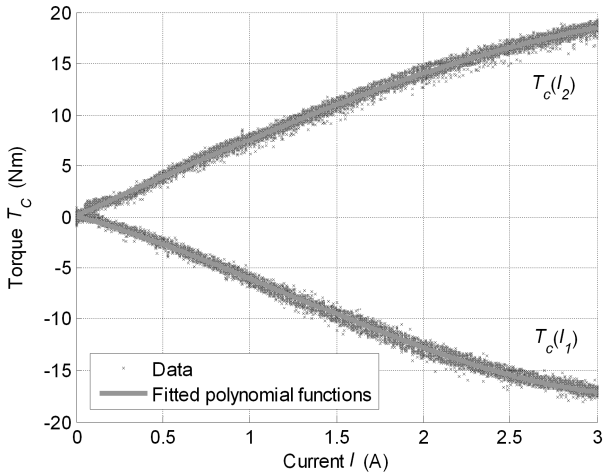

Fig. 13 Torque output function of brake currents and fitted third order polynomial functions.

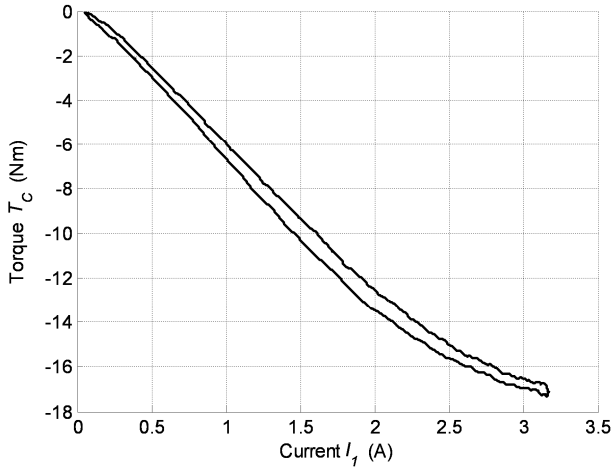

Fig. 14 Torque output function of current in brake 1.

The torque controller, making use of the inverse of the identified polynomial relationships $T_C(I_1)$ and $T_C(I_2)$ (see Fig. 13) is presented in Fig. 15. According to the torque command T_{Cref}, the controller generates the brake current commands I_{1ref} and I_{2ref} which are communicated to the corresponding current drives. Due to the resistive-inductive nature of the brake electrical circuit, a few milliseconds are then required for these currents to establish. Note that no attempt was made to compensate for the hysteretic nature of the torque response, which only causes deviations of up to 0.5 Nm between the command and the actual output. We believe that this is compatible with most applications. However, compensation techniques could be implemented (e.g., [54]).

With this controller in place, the open-loop torque tracking performances were tested. Fig. 16 illustrates a rapidly varying sinusoidal command concurrently with the torque measured through the fixed sensor, showing that fast and accurate torque tracking is possible.

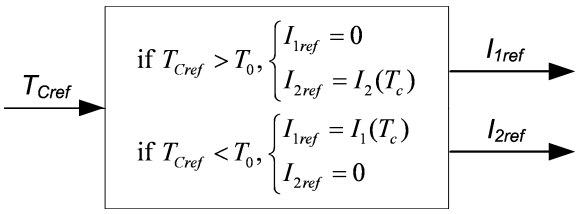

Fig. 15 Current feed-forward torque control scheme.

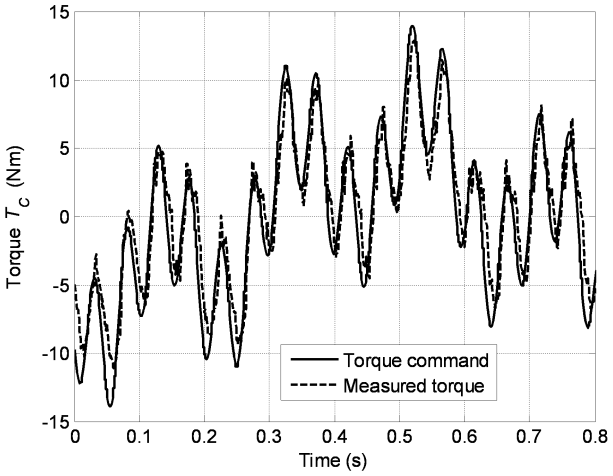

Fig. 16 Torque tracking with T_{Cref} = 5sin(2πt) + 5sin(5*2πt) + 5sin(20*2πt).

To better capture torque generation performances, 10 and 15 Nm sinusoidal torque commands sweeping from 0 to 40 Hz were applied. Transfer function identification techniques were then used to reveal the performances shown in Fig. 17. Using a 3 dB power loss cutoff frequency definition, it is apparent that the bandwidth is greater than 40 Hz. The figure also reveals that the performance is dependant of the magnitude of commands at high frequencies. However, to simplify discussions, the system is hereafter treated as linear with the torque command (T_{Cref}) to torque output (T_C) transfer function, of which Fig. 17 is a visual representation, termed $G(s)$.

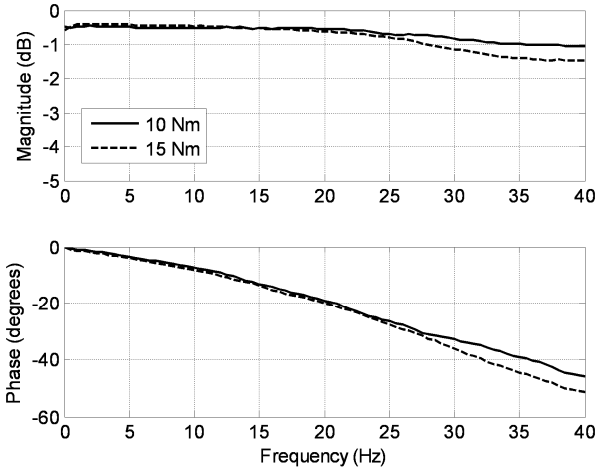

Fig. 17 Bode plot of the transfer function $G(s)$ between the commanded torque (T_{Cref}) and the measured output torque (T_C).

Using $G(s)$ and the previously identified intrinsic output impedance $Z_{out}(s)$, the expected torque output T_{out} during motion can be rewritten as in (7). This equation, which completely characterizes torque control performances, states that T_{out} is a combination of the open-loop controlled torque and of the actuator intrinsic resistance to motion.

$$\begin{cases} T_{out}(s) = G(s)T_{Cref}(s) - Z_{out}(s)\omega_{out}(s) \\ Z_{out}(s) = (1.2e^{-4}s + 0.01)\ \text{Nm.s/rad} \end{cases} \quad (7)$$

B. Interaction Control

Interaction control was performed using an impedance controller developed as shown in Fig. 18. As illustrated, the torque command $T_{Cref}(s)$ is modulated according to output motion $\omega_{out}(s)$ following a dynamically varying impedance relationship $Z_V(s)$. The open-loop torque controller then pilots the brakes. The resulting torque, which is also affected by the $Z_{out}(s)$ during motion, is applied to the load. In the diagram, this load is characterized by its admittance function $Y_e(s)$. To enable motion control, a reference position $\Theta_V(s)$ (with reference velocity $\omega_V(s)$) is given to the controller. Modifying this reference is equivalent to moving the virtual attach point of Z_V(s). A torque feed-forward can also be given to the controller through T_V. It can be used, for example, to compensate gravity acting on the actuated link. Finally, to accommodate safety constraints, the commanded torque is bounded between T_{max} and -T_{max}. Because the actuator has very low intrinsic output inertia, impact and interaction forces can be effectively limited by these bounds.

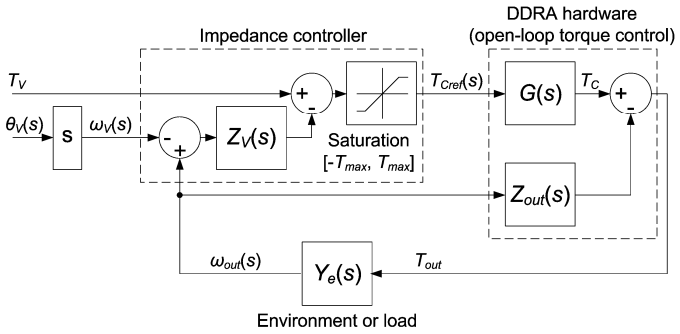

Fig. 18 Bloc diagram of the impedance controller.

The virtual impedance function $Z_V(s)$ used in the controller is detailed in (8). It is composed of three terms. They respectively emulate a mechanical spring with stiffness K_V, a mechanical damper with coefficient B_V and a position error integrator with gain I_V. This is similar to a PID controller. However, whereas a PID controller typically aims at regulating either torque or velocity, this controller aims at modulating the relationship between both. Another distinction is that the gains (K_V, B_V and I_V) can be changed in real time to continuously adapt the interaction behavior to the task. This gives the controller its versatility.

$$Z_V(s) = \frac{K_V}{s} + B_V + \frac{I_V}{s^2} \quad (8)$$

For stable interaction, it is important to know what range of virtual impedances can be commanded. This range is called the Z-width [15]. To illustrate this, the following experiment was conducted. The actuator was coupled to a small inertial load (0.008 kg.m^2) as shown in Fig. 19. Then, different virtual spring and damper combinations were commanded. For each pair, stability was considered achieved when, judging by the position curve, no sustained oscillation could be elicited. To implement damping, the output velocity ω_{out} was estimated using a backward differentiation of the output position and a first order low-pass filter. Tests were conducted using filters with 30 and 160 Hz cutoff frequencies. With the 160 Hz filter, tests were stopped at a damping of 8.5 Nm.s/rad because the haptic feeling was rapidly deteriorating. Results are shown in Fig. 20. The area under a curve represents the range of stable impedances while coupled to the small inertial load. Damping ratios (ζ) are also shown.

Haptic interfaces, for example, require such versatility. In this field, simulating the transition between free motion and stiff walls is a common benchmark. With the prototype, using a 20 cm radius manipulandum with an inertia of 0.008 kg.m^2 (Fig. 19), a transition between free motion and a stiffness of 30 N/mm (1200 Nm/rad) is feasible. This is enough to convey the presence of "hard" or "rigid" walls according to [55].

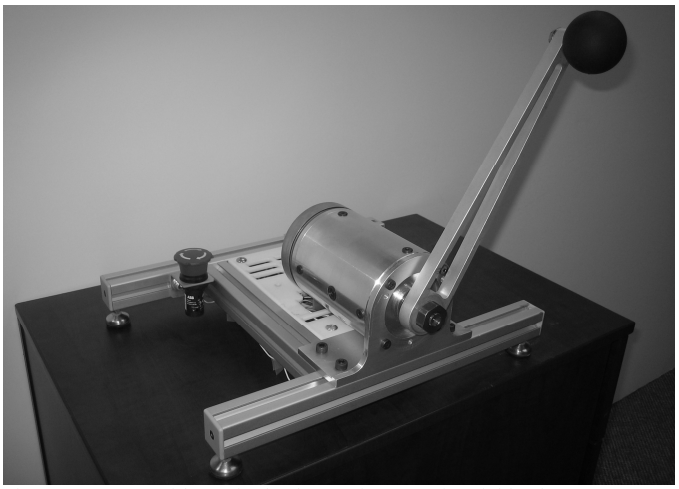

Fig. 19 Actuator with manipulandum acting as an inertial load.

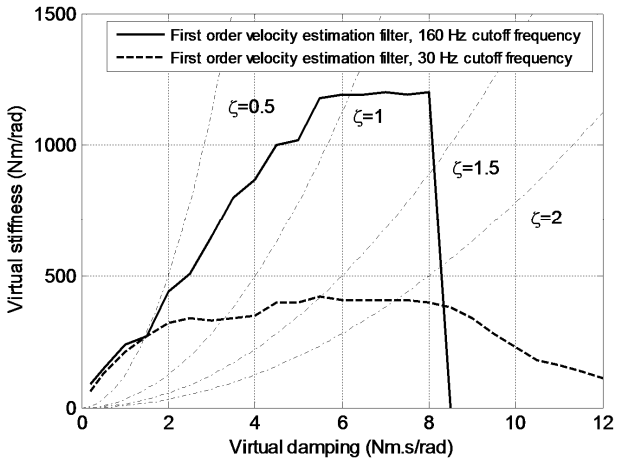

Fig. 20 Stable Z-width for interaction with an 0.008 kg.m^2 inertial load with damping ratios (ζ).

As a note, the Z-width shown in Fig. 20 is load specific. To be generalizable to unknown environments, further characterization is required. As mentioned, interaction stability can almost be guaranteed if the emulated impedance is passive. A conservative approach would thus be to identify the frequency dependant range of impedances that can be emulated passively and to respect these bounds during interaction. An example of such a characterization, using a dedicated test bench, can be found in [16].

C. Motion Control

The developed impedance controller can also be used for high performance motion control. For stiff motion tracking, the virtual impedance is set to a high but stable value and the desired trajectory is communicated through $\Theta_V(s)$ (and $\omega_V(s)$). Also, if the load is known, an approximation of the required torque can be feed-forwarded through T_V to improve performances. Fig. 21 illustrates the results of a motion tracking experiment, showing that fast and precise motion is possible. This is in part because of the actuator zero backlash, low friction and low inertia.

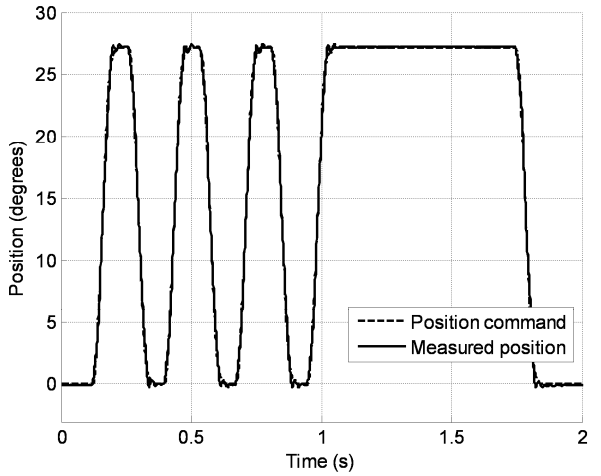

Fig. 21 Position tracking, 0.008 kg.m^2 inertial load, K_V = 575 Nm/rad, B_V = 4 Nm.s/rad and I_V = 3 Nm/(rad.s).

VII. Discussion

To enable improved physical interaction capabilities, the DDRA objectives were to achieve high torque density, low intrinsic impedance, high force bandwidth and high fidelity force control. Using those metrics, Table II compares the performances of our prototype with available high performance EM actuators.

TABLE II
Performance Comparison

	DDRA prototype	Geared motors[1]	Direct drive motors[2]
Nominal torque density (Nm/kg)	5	3 to 28	2 to 7
Torque to inertia ratio (Nm/kg.m^2)	93 220	4 to 209	1899 to 8081
Torque bandwidth (Hz)	>40	N.A.	N.A.
High fidelity force control	Yes[3]	No	Yes

1- RHS/RFS, RFK, RSF and FHA-C series by Harmonic Drive.
2- TML and TMM series by Etel, diameters up to 290 mm. No housing, bearing or feedback device.
3- Torque imprecision equivalent to ±2.5% of the full range.

1) *Torque density*. The torque density of the DDRA prototype is arguably superior to the one of complete direct drive motor solutions (with housings, bearings and feedback devices). However, the one of high performance geared motors remains superior. Torque density is part of the reason why geared motors have become the common actuator choice for serial robotic manipulators. This suggests that before it can be used in such manipulators, the DDRA torque density should be improved. One way is to use higher reduction ratios between the motor and the output to enable a reduction of the velocity source motor mass. This is possible because the prototype achieves 160 rpm (Table I) whereas joint speeds exceeding 30 to 45 rpm are seldom required for robotic manipulators. Further optimization of the MR brakes mass should also be investigated.

2) *Intrinsic impedance*. Table II shows that, among available EM actuators, the inertia of the DDRA prototype is exceptionally small. The intrinsic damping (not reported in the table) is also very small. This leads to an actuator with almost transparent dynamics.

3) *Torque bandwidth*. The torque control bandwidth of the DDRA prototype is greater than 40 Hz. This is substantial compared to the 7 Hz upper limit for humans [39]. No bandwidth data were available for EM motors of Table II, but, as a reference, it is typically less than 100 Hz for direct drive motors [44]. Higher performances are possible with low inductance designs. A large bandwidth enables the emulation of stiffer impedances. Yet, it has been shown that an intrinsic damping also contributes significantly [15]. For this reason, a performance metric encompassing the effects of bandwidth and intrinsic impedance could be useful in the future. This could be the frequency dependant passive Z-width [16].

4) *Force control fidelity*. Contrasting with most geared motors, the DDRA prototype is able of precise torque generation (Fig. 16). Nonetheless, two detrimental phenomena occur. The first is torque hysteresis (Fig. 14) probably caused by magnetic remanence in the brakes. However, because care was taken in the design, it is relatively small and causes a

maximum deviation of 0.5 Nm from the modeled torque versus currents relationships. The second phenomenon, probably caused by a magnetic gradient induced particle migration in the brakes, is that the measured torque tends to increase slowly through long trials to eventually stabilize at a maximum of about 0.5 Nm above the command. Both phenomena thus create a possible deviation of 1 Nm from the torque command, which represents 2.5% of the ±20 Nm range. We believe that this is compatible with most robotic physical interaction scenarios.

The objective to develop an actuator suited for physically interacting robotic systems led to a solution with low friction, very inertia and zero backlash. These same characteristics also make the DDRA suitable for high performance motion. For example, when compared to geared motors, the DDRA low friction and eliminated backlash contribute to increase positioning precision (Fig. 21). Also, the DDRA low inertia leads to improved dynamic performances. Indeed, to optimize the acceleration capabilities of a geared motor, the speed reduction ratio should be chosen so that the actuator inertia matches the one of the load. Half of the torque then accelerates the motor rotor whereas only half goes to the load. With a DDRA built from the same motor and with the same reduction ratio, achievable accelerations are almost doubled because the actuator inertia is negligible. Moreover, until speed requirements become an issue, higher reduction ratios can be used to even further increase acceleration capabilities.

VIII. Conclusion

To address the physical interaction limitations of current robotic systems, this paper introduced a novel actuator concept based on the synergistic use of an EM motor and two differentially coupled MR brakes. As confirmed by our results, this approach enables the simultaneous achievement of high force density, low intrinsic impedance, high force bandwidth and precise force control, leading to a potential for safe, robust and highly versatile robotic interaction. We believe that, in the future, such actuators, designed to enable interaction, will contribute to increase the applicability and usability of robotic systems and help to address a number of relevant issues in domains ranging from manufacturing to health care.

References

[1] J. Wang, G. Zhang, H. Zhang and T. Fuhlbrigge, "Force control technologies for new robotic applications," in *Proceedings IEEE International Conference on Technologies for Practical Robot Applications*, 2008, pp. 143-149.

[2] A. Kochan, "Robots and operators work hand in hand," in *Industrial Robot: an International Journal*, vol. 33, 2006, pp. 422-424.

[3] J. Wang, H. Zhang and G. Zhang, "A force control assisted robot path generation system," in *Proceedings 4th IEEE Conference on Automation Science and Engineering*, 2008, pp. 528-533.

[4] R. Riener, M. Frey, M. Bernhardt, T. Nef and G. Colombo, "Human-centered rehabilitation robotics," in *Proceedings IEEE 9th International Conference on Rehabilitation Robotics*, 2005, pp. 319-322.

[5] H. Vallery, J. Veneman, E. van Asseldonk, R. Ekkelenkamp, M. Buss and D. K. van, "Compliant actuation of rehabilitation robots," in *IEEE Robotics and Automation Magazine*, vol. 15, 2008, pp. 60-69.

[6] K. A. Wyrobek, E. H. Berger, D. L. Van and J. K. Salisbury, "Towards a personal robotics development platform: Rationale and design of an intrinsically safe personal robot," in *Proceedings IEEE International Conference on Robotics and Automation*, 2008, pp. 2165-2170.

[7] W. Song, H. Lee and Z. Bien, "KARES: Intelligent wheelchair-mounted robotic arm system using vision and force sensor," in *Robotics and Autonomous Systems*, vol. 28, 1999, pp. 83-94.

[8] I. Vanderniepen, R. Van Ham, M. Van Damme and D. Lefeber, "Design of a powered elbow orthosis for orthopaedic rehabilitation using compliant actuation," in *Proceedings International Conference on Biomedical Robotics and Biomechatronics*, 2008, pp. 801-806.

[9] A. De Santis, B. Siciliano, A. De Luca and A. Bicchi, "An atlas of physical human-robot interaction," in *Mechanism and Machine Theory*, vol. 43, 2008, pp. 253-270.

[10] A. Bicchi, M. A. Peshkin and J. E. Colgate, "Safety for physical human-robot interaction," in *Springer Handbook of Robotics*, B. Siciliano and O. Khatib, 2008, pp. 1335-1348.

[11] S. Haddadin, A. Albu-Schaffer, M. Frommberger and G. Hirzinger, "The role of the robot mass and velocity in physical human-robot interaction - parts I and II," in *Proceedings IEEE International Conference on Robotics and Automation*, 2008, pp. 1331-1345.

[12] M. Zinn, O. Khatib, B. Roth and J. K. Salisbury, "Playing it safe," in *IEEE Robotics and Automation Magazine*, vol. 11, 2004, pp. 12-21.

[13] N. Hogan, "Impedance control: an approach to manipulation. Parts I, II and III," in *Transactions of the ASME. Journal of Dynamic Systems, Measurement and Control*, vol. 107, 1985, pp. 1-24.

[14] N. Hogan and S. P. Buerger, *Robotics and Automation Handbook*, Chapter 19: Impedance and Interaction Control, Boca Raton: CRC Press, 2005, pp. 19.1-19.24.

[15] J. E. Colgate and J. M. Brown, "Factors affecting the Z-width of a haptic display," in *Proceedings IEEE International Conference on Robotics and Automation*, 1994, pp. 3205-3210.

[16] D. W. Weir, J. E. Colgate and M. A. Peshkin, "Measuring and increasing Z-width with active electrical damping," in *Symposium on Haptics Interfaces for Virtual Environment and Teleoperator Systems*, 2008, pp. 169-175.

[17] J. E. Colgate and N. Hogan, "Robust control of dynamically interacting systems," *International Journal of Control*, vol. 48(1), 1988, pp. 65-88.

[18] E. Colgate and N. Hogan, "Analysis of contact instability in terms of passive physical equivalents," in *Proceedings IEEE International Conference on Robotics and Automation*, 1989, pp. 404-409.

[19] W. S. Newman, "Stability and performance limits of interaction controllers," in *Journal of Dynamic Systems, Measurement and Control, Transactions of the ASME*, vol. 114, 1992, pp. 563-570.

[20] S. P. Buerger, "Stable, High-Force, Low-Impedance Robotic Actuators for Human-Interactive Machines", Ph.D. dissertation, Massachusetts Institute of Technology, Cambridge, Boston, 2005.

[21] J. M. Hollerbach, I. W. Hunter and J. Ballantine, "A comparative analysis of actuator technologies for robotics," *The Robotics Review* 2, 1992, pp. 299-342.

[22] R. W. Armstrong, "Load to motor inertia mismatch: unveiling the truth," presented at *Drives Control Conference*, Telford, England, 1998.

[23] N. Hogan, H. I. Krebs, J. Charnnarong, P. Srikrishna and A. Sharon, "MIT-MANUS: A workstation for manual therapy and training. I," in *Proceedings IEEE International Workshop on Robot and Human Communication*, 1992, pp. 161-165.

[24] J. K. Salisbury, W. T. Townsend, "Compact cable transmission with cable differential," U.S. Patent 5 207 114, May 4, 1993.

[25] D. Vischer and O. Khatib, "Design and development of high-performance torque-controlled joints," in *IEEE Transactions on Robotics and Automation*, vol. 11, 1995, pp. 537-5445.

[26] S. D. Eppinger and W. P. Seering, "Understanding bandwidth limitations in robot force control," in *Proceedings IEEE International Conference on Robotics and Automation*, 1987, pp. 904-909.

[27] G. Hirzinger, N. Sporer, M. Schedl, J. Butterfass and M. Grebenstein, "Torque-controlled lightweight arms and articulated hands: Do we reach technological limits now?" in *International Journal of Robotics Research*, vol. 23, 2004, pp. 331-340.

[28] A. Albu-Schaffer, O. Eiberger, M. Grebenstein, S. Haddadin, C. Ott, T. Wimbock, S. Wolf and G. Hirzinger, "Soft robotics," *IEEE Robotics and Automation Magazine*, vol. 15, 2008, pp. 20-30.

[29] M. M. Williamson, "Series Elastic Actuators", Ph.D. dissertation, Massachusetts Institute of Technology, Boston, 1995.
[30] D. W. Robinson, "Design and Analysis of Series Elasticity in Closed-Loop Actuator Force Control," Ph.D. dissertation, Massachusetts Institute of Technology, Boston, 2000.
[31] M. Lauria, M. Legault, M. Lavoie and F. Michaud, "Differential elastic actuator for robotic interaction tasks," in *IEEE International Conference on Robotics and Automation*, 2008, pp. 3606-3611.
[32] A. Edsinger-Gonzales and J. Weber, "Domo: A force sensing humanoid robot for manipulation research," in *Proceedings IEEE/RAS International Conference on Humanoid Robots*, 2004, pp. 273-91.
[33] J. B. Morrell, "Parallel Coupled Micro-Macro Actuators," Ph.D. dissertation, Massachusetts Institute of Technology, Boston, 1996.
[34] M. Zinn, O. Khatib, B. Roth and J. K. Salisbury, "Large workspace haptic devices - A new actuation approach," in *Proceedings Symposium on Haptics Interfaces for Virtual Environment and Teleoperator Systems*, 2008, pp. 185-192.
[35] G. Tonietti, "Variable Impedance Actuation, A Co-Design Solution to the Safety/Performance Tradeoff in Physical Human-Robot Interaction," Ph.D. dissertation, University of Pisa, Italy, 2005.
[36] R. Schiavi, G. Grioli, S. Sen and A. Bicchi, "VSA-II: A novel prototype of variable stiffness actuator for safe and performing robots interacting with humans," in *Proceedings IEEE International Conference on Robotics and Automation*, 2008, pp. 2171-2176.
[37] S. Wolf and G. Hirzinger, "A new variable stiffness design: Matching requirements of the next robot generation," in *Proceedings IEEE International Conference on Robotics and Automation*, 2008, pp. 1741-1746.
[38] W. Zhou, C. Chew and G. Hong, "Property analysis for series MR-fluid damper actuator system," in *Proceedings IEEE Conference on Robotics, Automation and Mechatronics*, 2004, pp. 560-565.
[39] D. Chapuis, "Application of Ultrasonic Motors to MR-Compatible Haptic Interfaces", Ph.D. dissertation, École polytechnique fédérale de Lausanne, Lausanne, Switzerland, 2009.
[40] M. Sakaguchi and J. Furusho, "Development of ER actuators and their applications to force display systems," in *Proceedings IEEE Virtual Reality Annual International Symposium*, 1998, pp. 66-70.
[41] S. B. Choi, S. S. Han, H. K. Kim and C. C. Cheong, "H $_{\text{infinity}}$ control of a flexible gantry robot arm using smart actuators," in *Mechatronics*, vol. 9, 1999, pp. 271-286.
[42] H. Hakogi, M. Ohaba, N. Kuramochi and H. Yano, "Torque control of a rehabilitation teaching robot using magneto-rheological fluid clutches," in *JSME international journal*, series B, vol. 48, 2006, pp. 501-507.
[43] A. R. Johnson, W. A. Bullough and J. Makin, "Dynamic simulation and performance of an electro-rheological clutch based reciprocating mechanism," *Smart Materials and Structures*, vol. 8, 1999, pp. 591-600.
[44] J. L. Pons, *Emerging Actuator Technologies: A Micromechatronic Approach*, Chichester England: Wiley, 2005, ch. 7.
[45] X. Wang and F. Gordaninejad, "Magnetorheological materials and their applications," in *Intelligent Materials*, M. Shahinpoor and H.-J. Schneider, Cambridge England: RSC Publishing, 2008, pp. 339-385.
[46] M. R. Jolly, J. W. Bender and J. D. Carlson, "Properties and applications of commercial magnetorheological fluids," *Journal of Intelligent Materials, Systems and Structures*, vol. 10, n1, pp. 5-13, 1999.
[47] B. Kavlicoglu, F. Gordaninejad, C. Evrensel, A. Fuchs and G. Korol, "A semi-active, high-torque, magnetorheological fluid limited slip differential clutch," *Journal of Vibrations and Acoustics,* vol. 128, 2006, pp. 604-610, 2006.
[48] B. Deffenbaugh, H. Herr, G. Pratt and M. Wittig, "Electronically controlled prosthetic knee," U.S. Patent 6 764 520, July 20, 2004.
[49] W. Szelag, P. Sujka and R. Walendowski, "Field-circuit transient analysis of a magnetorheological fluid brake," *International Journal for Computation and Mathematics in Electrical and Electronic Engineering,* vol. 23, pp. 986-995, 2004.
[50] B. Liu, W. H. Li, P. B. Kosasih and X. Z. Zhang, "Development of an MR-brake-based haptic device," *Smart Materials and Structures*, v 15, n 6, p 1960-6, 2006.
[51] C. Gabriel, H. M. Laun, G. Schmidt, G. Ötter, C. Kieburg, J. Pfister, "Migration phenomena in magnetorheometry and MR-applications," in *Proceedings of Actuator 11th International Conference and Exhibition on New Actuators and Drive Systems*, 2008, pp. 489-490.
[52] D. Lampe, A. Thess and C. Dotzauer, "MRF-clutch-design considerations and performance," in *Proceedings of Actuator 6th International Conference on New Actuators*, 1998, pp. 449-453.
[53] P. Fauteux, M. Lauria, M. Legault, B. Heintz and F. Michaud, "Dual differential rheological actuator for robotic interaction tasks," in *Proceeding IEEE/ASME International Conference on Advanced Intelligent Mechatronics*, 2009, pp. 47-52.
[54] J. Maas, K. Voth, A. Wiehe and C. Graf, "Realtime compensation methods for hysteresis based magnetorheological actuators," in *2009 IEEE/ASME International Conference on Advanced Intelligent Mechatronics*, 2009, pp. 1010-15.
[55] H. Z. Tan, B. Eberman, M. A. Srinivasan and B. Cheng, "Human factors for the design of force-reflecting haptic interfaces," in *Proceedings International Mechanical Engineering Congress and Exposition*, 1994, pp. 353-359.

Philippe Fauteux received his Bachelor's degree in mechanical engineering in 2007 form the Université de Sherbrooke, Québec, Canada, where he currently is a candidate for the Master's degree in mechanical engineering and a member of the Intelligent, Interactive, Integrated and Interdisciplinary Robot Lab (IntRoLab) team. His current research interests include the design and control of robotic systems with an emphasis on physically interacting machines.

Michel Lauria received his M.Sc. in Micro-engineering in 1997 and his Doctoral degree in 2003 from the Swiss Federal Institute of Technology (EPFL). From 2003 to 2009, he was a Professor at the Department of Electrical Engineering and Computer Engineering of the Université de Sherbrooke, Québec, Canada. Since 2009, he is a Professor at the University of Applied Sciences Western Switzerland (HES-SO). His research interests are in robotic design and control, mechatronics and high-performance actuators.

Benoît Heintz received his Master's of Science in electronics, robotics and industrial computing at Polytech'Montpellier, France in 2008. Since 2007, he is a candidate for the Master's degree in electrical engineering at the Université de Sherbrooke, Québec, Canada, as a member of IntRoLab.

François Michaud (M'90) received his bachelor's degree ('92), Master's degree ('93) and Ph.D. degree ('96) in electrical engineering from the Université de Sherbrooke, Québec Canada.

After completing postdoctoral work at Brandeis University, Waltham MA ('97), he became a faculty member in the Department of Electrical Engineering and Computer Engineering of the Université de Sherbrooke, and founded IntRoLab (formerly LABORIUS), a research laboratory working on designing intelligent autonomous systems that can assist humans in living environments. His research interests are in architectural methodologies for intelligent decision-making, design of autonomous mobile robots, social robotics, robots for children with autism, robot learning and intelligent systems.

Prof. Michaud is the Canada Research Chairholder in Mobile Robots and Autonomous Intelligent Systems, and the Director of the Centre of Excellence on Information Engineering. He is a member of IEEE, AAAI and OIQ (Ordre des ingénieurs du Québec). In 2003, he received the Young Engineer Achievement Award from the Canadian Council of Professional Engineers.